Desalination and Water Treatment
www.deswater.com

doi:10.5004/dwt.2019.24687

169 (2019) 294–304
November

Improving the removal of chromium by polymer epichlorohydrin-dimethylamine functionalized mesoporous silica

Shanshan Zhang[a], Xing Xu[a], Qinyan Yue[a,*], Wengang Wang[b], Baoyu Gao[a,*]

[a]*Shandong Provincial Key Laboratory of Water Pollution Control and Resource Reuse, School of Environmental Science and Engineering, Shandong University, Qingdao, 266237, China, emails: qyyue58@aliyun.com (Q.Y. Yue), bygao@sdu.edu.cn (B.Y. Gao), zhangshanshan113@163.com (S.S. Zhang), xuxing@sdu.edu.cn (X. Xu)*
[b]*Shandong Academy of Environmental Science, Jinan 250100, China, email: 18366106770@163.com*

Received 23 January 2019; Accepted 8 July 2019

ABSTRACT

The cationic polymer epichlorohydrin-dimethylamine (EPI-DMA) was first employed as the modifier for preparing the SiO_2@EPI-DMA by sonochemical in situ modification. The functionalized mesoporous silica (SiO_2@EPI-DMA) was then used for removing Cr(VI) from the aqueous environment. The result showed that EPI-DMA had been grafted to a certain extent, improving the positive charge of SiO_2. The adsorption capacity of SiO_2@EPI-DMA for Cr(VI) was improved by electrostatic attraction. The XPS results also indicated that the Cr(VI) was partially reduced to Cr(III), which indicated that the redox reaction also contributed to the Cr(VI) removal. The Langmuir isotherm model was suitable to describe Cr(VI) adsorption equilibrium data by SiO_2@EPI-DMA, and the adsorption kinetics data were depicted quite well by the pseudo-second-order. The maximum monolayer adsorption capacity of SiO_2@EPI-DMA was about 102.7 mg g^{-1}, which was greatly higher than that of neat SiO_2. It indicates that the EPI-DMA is a promising functional reagent available.

Keywords: Functionalized mesoporous silica; Polymer epichlorohydrin-dimethylamine; Chromium; Sonochemical in situ modification

1. Introduction

Heavy metals have accumulated hazards to animals and human beings due to food chains [1]. Heavy metals include anions and cationic pollutants. Among others, chromium is a major anionic heavy metal pollutant originating from industrial discharges such as textile factories, paper production, petroleum refining, electroplating and wood preservation process [2]. Recently, several techniques have been applied for removing Cr(VI) from the aqueous environment, for example, oxidation–reduction process [3], classified precipitation process [4], adsorption and biological methods [5]. Among others, adsorption is the most frequently used technique because of its simplicity in design and operation [4]. Various materials [6–11], such as bio-sorbents, zeolites, chitosan and activated carbon have been widely applied to purify heavy metals sewage [5,12,13]. Furthermore, it has drawn more attention to develop low-cost and efficient functionalized mesoporous silica adsorbents.

Considering the promising properties (e.g., tunable pore size, easily doped unstructured skeleton and high surface area) of mesoporous silica [14,15], the distinguished mesoporous silica nanoparticles have been applied in biosensors, electronics, medicine, catalyst, adsorbents, cosmetics and peptides separation [16–19]. Owing to the presence of abundant hydroxyl groups, neat mesoporous silica nanoparticles in aqueous solution always showed weak negativity potential, which exhibited good affinity for different cationic metal pollutants, such as copper, lead and zinc ions [20,21].

* Corresponding author.

However, mesoporous silica nanoparticles lack sufficient specific sites for adsorbing anionic heavy metal pollutants such as dichromate anions ($Cr_2O_7^{2-}$). Therefore, immobilization of appropriate chemical groups for mesoporous silica has attracted much attention for the purpose of enhancing the removal of Cr(VI) [22].

Functional mesoporous silica materials have been prepared with some groups. For instance, a series of polymers, such as polyvinyl chloride (PVC), polyethylene glycol (PEG), polyvinyl alcohol (PVA) have been adopted to modify the mesoporous silica [19,23,24]. Li et al. [25] reported 3-aminopropyltrimethoxysliane grafted mesoporous silica for removal of Cr(VI). Polymer epichlorohydrin-dimethylamine (EPI-DMA) is a poly quaternary with strong-cation electrolyte, which could be used as a cationic functional agent. The EPI-DMA has displayed good hydrolysis stability and high cation density [26]. However, there has been little information that the mesoporous silica supported the EPI-DMA for uptake of Cr(VI).

Ultrasound has proved a useful method for shortening the reaction time due to acoustic cavitation [27–29], which is the foaming process of production, growth and implosive collapse in aqueous medium [30]. Under exposure to the penetration of sound field, the foam can be compressed and expanded at a very high rate, resulting in a high pressure. This high pressure will lead to a high chemical reactivity to accelerate the process [31]. Deka et al. [27] reported on the compound of ordered benzene-bridged PMOs by ultrasound. Seon et al. [32] have successfully synthesized Ti-SBA-15 by ultrasonic technique. The sonochemical in situ modification is an effective and facile method, which is generally applied in functionalization process.

The purpose of this study was to modify the mesoporous silica using cationic poly epichlorohydrin-dimethylamine (EPI-DMA) by sonochemical in situ modification for improving the Cr(VI) uptake. The modification conditions were studied on the basis of EPI-DMA grafting amount. The SiO_2@EPI-DMA was measured by SEM, TEM, N_2 adsorption/desorption, FTIR, zeta potential and XPS. Batch sorption experiments were conducted under various pH and dosage operational conditions. Meanwhile, the adsorption isotherm as well as the kinetics of anionic Cr(VI) by SiO_2@EPI-DMA was evaluated to ascertain the adsorption behavior and mechanism.

2. Experimental

2.1. Chemicals

Tetraethyl orthosilicate (TEOS), cetyltrimethylammonium bromide (CTAB) and ammonium hydroxide were purchased from Tianjin Kemiou Chemical Reagent Co. Ltd., (11 Xingyuan road, Xianshuigu industrial park, Tianjin, China). These reagents were of analytical grade. Poly epichlorohydrin-dimethylamine (EPI-DMA) was supplied by Shandong Binzhou Jiayuan Environmental Protection Co., Ltd., (560 Huanghewulu, Binzhou, Shandong, China). Potassium dichromate ($K_2Cr_2O_7$) was a guaranteed reagent which was obtained from Tianjin Guangfu Technology Development Co. Ltd., (29 Huachengzhonglu, Caozili Township, Wuqing District, Tianjin, China). Deionized water was applied throughout the experiments for dissolving operation. Various concentrations of Cr(VI) solutions were diluted with distilled water. All standard solutions for calibration of Cr(VI) concentration were prepared with deionized water.

2.2. Synthesis of SiO_2@EPI-DMA

First, the SiO_2 was synthesized with TEOS and CTAB by ultrasound-assisted procedure. In the synthesis process, 1.5 g CTAB was dissolved to 140 mL of distilled water, and 5 mL aqueous ammonia (25%) was added to the solution. After 15 min of irradiation, 6.5 mL TEOS was added dropwise into the homogeneous solution and constantly stirred under ultrasonic irradiation (50 W; cup horn: 40 kHz). The solid was collected after centrifugation (10,000 rpm). It was then washed with water until the pH reached 7.0. The primary material was dried and calcined at a ramp rate of 20°C/min up to 600°C in the muffle oven. The temperature was maintained for 6 h and then the synthesized SiO_2 was obtained.

Afterwards, the SiO_2@EPI-DMA samples were prepared with the ultrasound as shown in Fig. 1. Pure SiO_2 was dried for 2 h at 110°C to remove the surface-adsorbed water, and 2 g of SiO_2 was dispersed into a solution containing a given concentration of EPI-DMA. The compound was exposed to an ultrasound device (50 W; cup horn: 40 kHz). Subsequently, the sample was filtered and dried at 60°C in vacuum oven. The sorbent was then ground and pounded to splinters of 0.02–0.5 cm with small porcelain mortar, marked as SiO_2@

Fig. 1. Preparation of SiO_2@EPI-DMA; the structural formula of EPI-DMA.

EPI-DMA-1, SiO_2@EPI-DMA-2, SiO_2@EPI-DMA-3, SiO_2@EPI-DMA-4 and SiO_2@EPI-DMA-5, respectively, according to the various concentrations of EPI-DMA (1%, 2%, 5%, 10%, 15%).

2.3. Physicochemical characterization

Textural analysis was conducted with a surface area analyzer (JWBK 122W, Beijing JWCB Sci & Tech Co., Ltd., China), at 77 K. The surface area (S_{BET}) and distribution of pore size were determined by the density functional theory method and the BET equation from the N_2 adsorption/desorption isotherm data in relative pressures (P/P_0: 0.05–0.3). TEM, SEM and EDS were obtained with the JEM-1011 and HITACHI (Japan), S-4160 microscope. The surface chemical functional groups and adsorptions of SiO_2@EPI-DMA were analyzed by FTIR. The wavelength was recorded as from 4,000 to 400 cm^{-1}. Zeta potential was determined with JS94H Zeta (Shanghai Zhongchen, Shanghai, China). The surface binding states of SiO_2@EPI-DMA and Cr(VI) exhausted SiO_2@EPI-DMA (SiO_2@EPI-DMA(Cr)) samples were measured using X-ray photoelectron spectrometer (Axis Ultra DLD, Shimadzu-Kratos, UK).

2.4. Measure of grafting amount EPI-DMA

The content of EPI-DMA loaded on the surface of silicon could be measured by the high temperature burning reaction, which was represented by the loss of ignition, marked as *S*. The modified material was dried in drying oven at 110°C. The weight of the sample was accurately weighed and recorded as W_a (g). The samples were calcined for 4 h in the 600°C muffle furnace. Then, the sample was cooled in a dryer. The weight of the calcined sample was accurately weighed and recorded as W_b (g). The loss on ignition *S* was calculated according to Eq. (1) [33]:

$$S\left(\text{mg g}^{-1}\right)=\left(W_a-W_b\right)\times\frac{1{,}000}{W_a} \tag{1}$$

2.5. Static adsorption experiment

The investigation was to evaluate the adsorption of the Cr(VI) by SiO_2@EPI-DMA nanoparticles. The effects of nanoparticle dosages and pH were investigated. The pH of the Cr(VI) solution was varied from 2.0 to 12.0, and the adsorbent dosage and initial Cr(VI) concentration were maintained at 0.5 g L^{-1} and 25 mg L^{-1}. The adsorbent dosages were adjusted between 0.5 and 1.5 g L^{-1}, and other adsorption conditions such as stirring speed, temperature, contact time and Cr(VI) concentration were kept at 150 rpm, 25°C, 24 h and 25 mg L^{-1}, respectively. For the purpose of isotherms study, the Cr(VI) solutions from 25 to 150 mg L^{-1} were prepared. After the adsorption reached equilibrium, the solution samples were filtered with Advantec of 0.45 μm. Solution samples were taken at various intervals to investigate adsorption kinetics and the initial concentration was set at 25 mg L^{-1}. The residual concentrations in the filtrate were measured using UV–Vis (ultraviolet-visible spectrophotometry). The adsorption capacity of adsorbent was then calculated according to Eq. (2).

$$q_e=\frac{\left(C_0-C_e\right)V}{m} \tag{2}$$

where C_0 and C_e are the initial and equilibrium Cr(VI) liquid phase (mg/L); V is the total volume of Cr(VI) (mL); m is the mass of the SiO_2@EPI-DMA (g).

3. Results and discussion

3.1. Effect of modification on SiO_2@EPI-DMA

3.1.1. Modification processing temperature

The modification conditions such as processing modification time, initial EPI-DMA and pH were kept at 12 h, 15% and pH 7.0. The SiO_2@EPI-DMA was synthesized at different modification temperature. The effect of processing temperature on the modification of SiO_2@EPI-DMA was investigated in Fig. 2a. The grafting EPI-DMA amount and Cr(VI) adsorption capacity gradually decreased as the modification processing temperature increased. It could be inferred that this was due to the combination of cationic EPI-DMA and mesoporous silica by weak van der Waals force [33]. The increased temperature was not conducive to the formation of weak covalent bonds between cationic EPI-DMA and silanol on mesoporous silica, which made the decline of grafting EPI-DMA amount and Cr(VI) adsorption capacity. The modification processing temperature was 25°C, and the grafting amount was 17.30 mg/g and Cr(VI) adsorption capacity was 28.8 mg/g. Therefore, the optimal modification processing temperature was 25°C.

3.1.2. Initial EPI-DMA concentration

The effect of initial EPI-DMA concentration on modification of SiO_2@EPI-DMA is shown in Fig. 2b. SiO_2@EPI-DMA was prepared by adding a certain mass of SiO_2 in different EPI-DMA concentrations. The modification conditions such as processing modification time, temperature and pH were kept at 12 h, 25°C and pH 7.0. The grafting amount of EPI-DMA on silica and adsorption capacity for Cr(VI) both increased. The increased initial EPI-DMA concentration promoted the formation of covalent bonds between silanol and EPI-DMA, which made the grafting EPI-DMA amount and Cr(VI) adsorption capacity increased. As the EPI-DMA concentration increased to 15%, the grafting amount was 17.70 mg/g and the adsorption capacity for Cr(VI) was 30.06 mg/g. According to the results, the optimal processing EPI-DMA concentration was 15% for Cr(VI) adsorption.

3.2. Characterization of SiO_2@EPI-DMA

3.2.1. Textural structure analysis

The surface and pore characteristics were obtained from the N_2 adsorption/desorption experiment. The results are shown in Table 1 and Fig. 3. According to Fig. 3a, the isotherms were type IV for unmodified SiO_2 and SiO_2@EPI-DMA [34], and these hysteresis loops were the type of H2 that were caused by the mesoporous structure [35]. As shown in Table 1, the decline of BET specific surface area was caused by the increased grafting EPI-DMA amount on

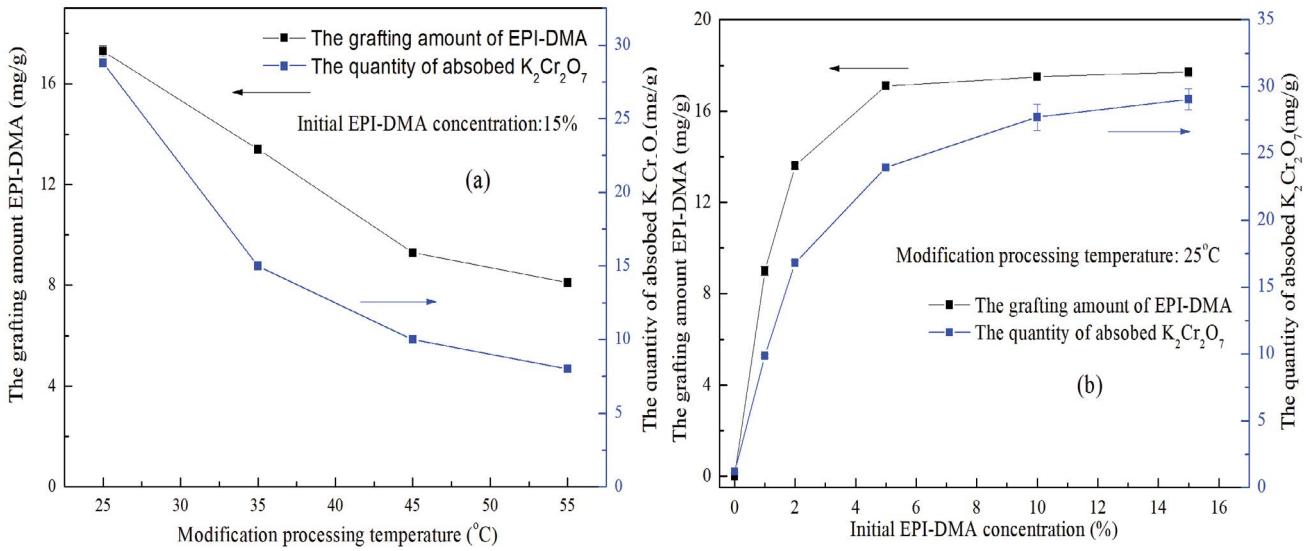

Fig. 2. (a) Effect of modification processing temperature and (b) initial EPI-DMA concentration on grafting amount of EPI-DMA and quantity of absorbed $K_2Cr_2O_7$.

Table 1
Textural characterization and grafting amount of the SiO_2@EPI-DMA

Sample	Specific surface area of BET (m^2/g)	Specific surface area of BJH (m^2/g)	Total pore volume (cm^3/g)	Pore diameter (nm)	Grafting amount EPI-DMA (mg/g)
SiO_2	1,040	1,310	1.277	4.913	0
SiO_2-EPI-DMA-1	916	998	0.749	3.267	9
SiO_2-EPI-DMA-2	899	920	0.643	3.259	13.6
SiO_2-EPI-DMA-3	646	804	0.526	3.253	17.1
SiO_2-EPI-DMA-4	473	464	0.378	3.191	17.5
SiO_2-EPI-DMA-5	310	320	0.334	3.011	17.7

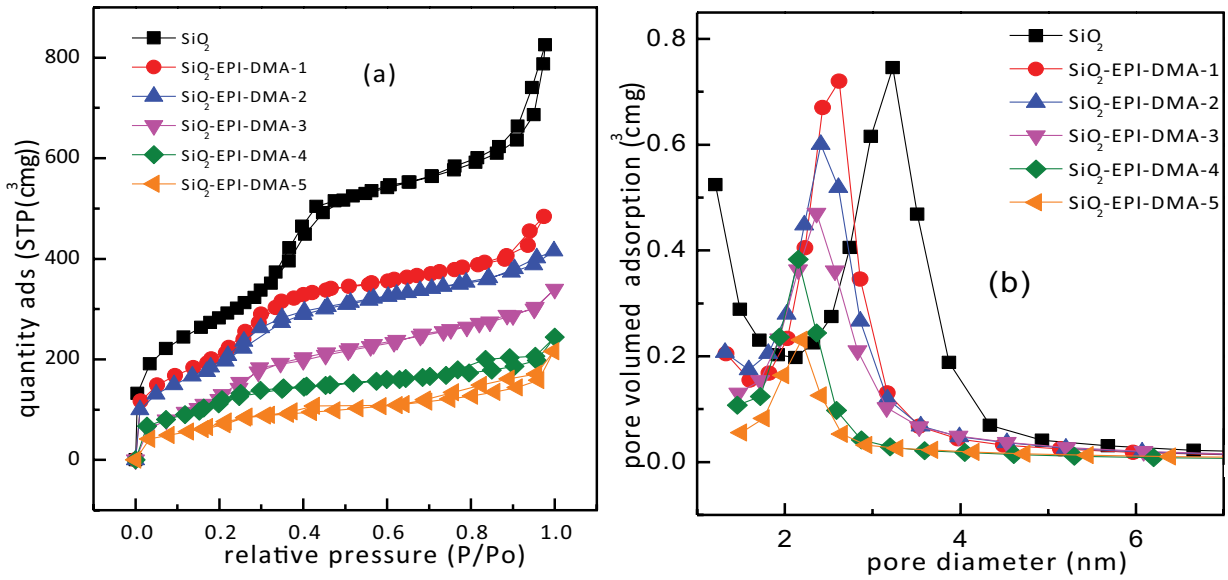

Fig. 3. (a) N_2 adsorption/desorption isotherms and (b) pore size distribution curves for SiO_2 and SiO_2@EPI-DMA samples.

the surface of SiO_2@EPI-DMA. The remarkable decrease of pore diameter and total pore volume was partially ascribed to the pore block of grafting EPI-DMA.

According to Fig. 2b, the increased grafting EPI-DMA amount improved the Cr(VI) adsorption, which indicated that the Cr(VI) adsorption did not rely on larger specific surface area, and mainly depended on electrical neutralization between positive EPI-DMA and negative Cr(VI). It proved that EPI-DMA was an effective modifying agent for SiO_2.

3.2.2. Zeta potential analysis

Surface charge of pure SiO_2 and SiO_2@EPI-DMA nanoparticles was evaluated by the micro-electrophoresis, and the results are as shown in Fig. 4. The zeta potentials of pure SiO_2 and SiO_2@EPI-DMA nanoparticles were measured by mixing 0.1 g samples with 50 mL of deionized water (pH 2.0–12.0). The zeta potential of pure SiO_2 decreased from +5 to –28 mV as the initial pH of the suspensions increased from 2.0 to 12.0, and the pH zero charge (pHPZC) point of the pure SiO_2 was located at 3.0. After the in situ modification, a more positively charged SiO_2@EPI-DMA sample was observed and the pH zero charge points (pHPZC) of SiO_2@EPI-DMA-1, SiO_2@EPI-DMA-2, SiO_2@EPI-DMA-3, SiO_2@EPI-DMA-4 and SiO_2@EPI-DMA-5 were located at 6.3, 7.9, 8.4, 8.5 and 8.7, respectively. It indicated that EPI-DMA was a good cationic modifier for SiO_2. The increased grafting EPI-DMA amount dramatically enhanced the amount of positive charge for SiO_2. The specific surface area and surface charge of SiO_2@EPI-DMA were most affected after modification. Therefore, SiO_2@EPI-DMA-5 with best adsorption capacity for Cr(VI) was employed in following characteristics tests.

3.2.3. FTIR analysis

The FTIR spectra of SiO_2 and SiO_2@EPI-DMA-5 nanoparticles were as shown in Fig. 5. The bands located at 1,082; 806; 456 cm^{-1} were attributed to the bending modes, asymmetric and symmetric stretching vibrations for Si–O–Si in the patterns [36]. The peaks at around 3,370 and 1,627 cm^{-1} indicated stretching vibration and bending mode in O-H groups of the surface silanol groups (Si–OH) [37]. The band observed at about 1,483 cm^{-1} was associated with the stretching mode of amination groups [38], which indicated that the SiO_2 was grafted with quaternary ammonium functional groups originated from EPI-DMA. The band around 893 cm^{-1} in the Cr exhausted SiO_2@EPI-DMA-5(Cr) corresponded to the Cr bond stretching [13], which indicated that Cr(VI) was combined with EPI-DMA on the surface of mesoporous nanoparticles. The peaks of silanol and quaternary ammonium functional groups were shifted and their intensity decreased in the spectra of SiO_2@EPI-DMA-5(Cr), which played an important role in Cr(VI) adsorption.

3.2.4. Morphology analysis

The morphological analysis was used by TEM and SEM images. Figs. 6a, b and d show the TEM images (MAG × 80,000) of SiO_2, EPI-DMA and forming the SiO_2@EPI-DMA-5. It is clear that the morphology of SiO_2 was nano-rod-like and was easily aggregated owing to the hydrogen interaction of silanol on the surface. EPI-DMA was chain-like. SiO_2@EPI-DMA was almost the same shape as SiO_2 particles, and the dispersion degree was increased. As a result, the incorporation of EPI-DMA on the SiO_2 particles did not affect particle morphology. According to the SEM images (MAG × 60,000), the surface of SiO_2@EPI-DMA-5 particles was smooth, not pile up on the surface, which confirmed that the nanomaterials had good homogeneity in shape and size and good dispersity. It was evidence that the SiO_2 particles acted as host and EPI-DMA was anchored onto the SiO_2 uniformly.

3.2.5. X-ray photoelectron spectra analysis

The surface chemical state and the interactions between SiO_2@EPI-DMA-5 and Cr(VI) were evaluated by X-ray photoelectron spectra analysis. The XPS spectra of pristine

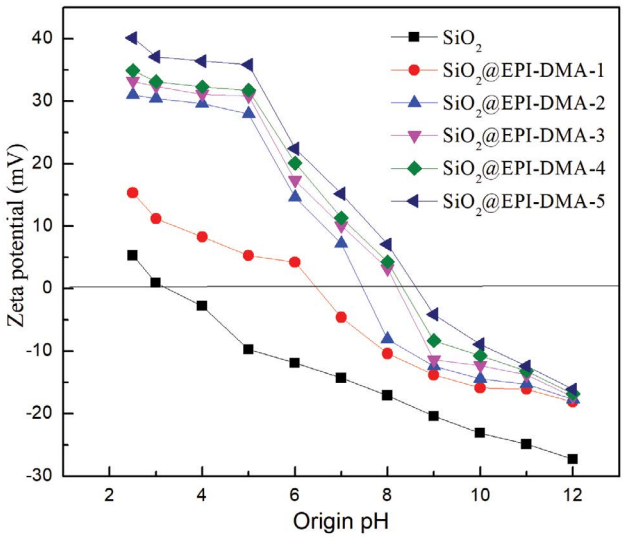

Fig. 4. Zeta potential of pure SiO_2 and SiO_2@EPI-DMA as a function of pH.

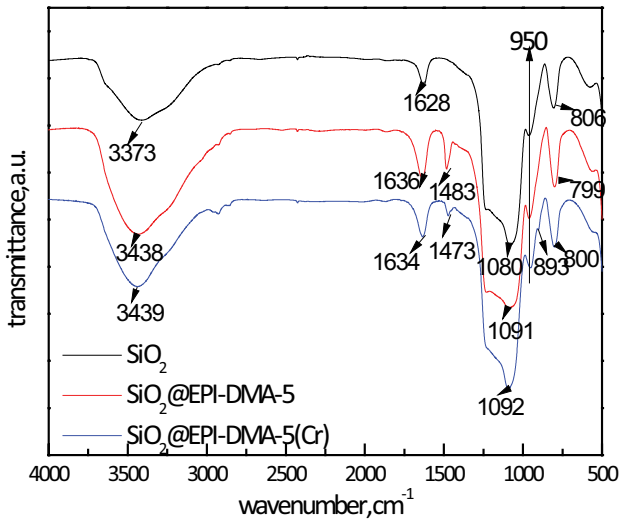

Fig. 5. FT-IR spectral curve of pure SiO_2, modified SiO_2@EPI-DMA-5, and adsorbed SiO_2@EPI-DMA-5(Cr).

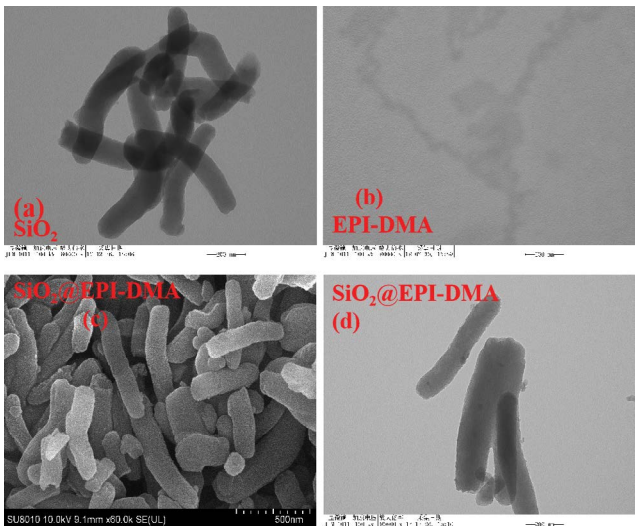

Fig. 6. TEM images of SiO_2 (a), EPI-DMA (b), MAG ×80,000; the SiO_2@EPI-DMA-5 of SEM images (c), MAG ×60,000 and TEM images (d), MAG ×80,000.

SiO_2@EPI-DMA-5 and saturated SiO_2@EPI-DMA-5(Cr) are shown in Fig. 7. It is obvious that the new binding energies around 578–587 eV were observed on the surface SiO_2@EPI-DMA-5(Cr), which revealed that the Cr(VI) was adsorbed on the SiO_2@EPI-DMA-5. As for the N 1s (398–403 eV) in Figs. 7b and d, the binding energies at 402 and 398 eV were assigned to the N^+ and C-N in the N1s spectra of SiO_2@EPI-DMA-5 and SiO_2@EPI-DMA-5(Cr), which indicated the grafted quaternary amine by EPI-DMA has no new peaks after adsorption. The Cr2p (569–597 eV) high resolution of SiO_2@EPI-DMA-5(Cr) is presented in Fig. 7c. The Cr2p1/2 and Cr2p3/2 were located at 578 and 587 eV. The Cr2p spectra were deconvoluted into four peaks, which were assigned to Cr(III)-OH (586.2 and 576 eV) and Cr(VI)-O (587.6 and 578.9 eV). It indicated that the chemisorption was involved in the adsorption process and Cr(VI) was reduced to less toxic Cr(III) by the silicone hydroxyl group [13].

Based on the above results of zeta potential and FTIR analysis, the proposed Cr(VI) adsorption mechanisms are presented in Fig. 8. It was initially that the electrostatic interactions between negative Cr(VI) ion and grafted positive EPI-DMA on the SiO_2@EPI-DMA, following by the ion exchange of Cl^- to Cr(VI) ions [39]. Afterwards, the reduction process occurred owing to the silicone hydroxyl group, which made the Cr(VI) reduced to Cr(III).

3.3. Batch sorption study

3.3.1. Effect of the pH on Cr(VI) adsorption

The effect of the pH on Cr(VI) equilibrium capacities for SiO_2@EPI-DMA adsorbents are shown in Fig. 9. When the pH was at 3.0–7.0, the species of Cr(VI) ions were mainly composed of $HCrO_4^-$ and $Cr_2O_7^{2-}$ [40]. The dosages, concentration of Cr(VI), contact time and adsorption temperature were kept at 0.5 g/L, 25 mg/L, 24 h and 25°C, respectively.

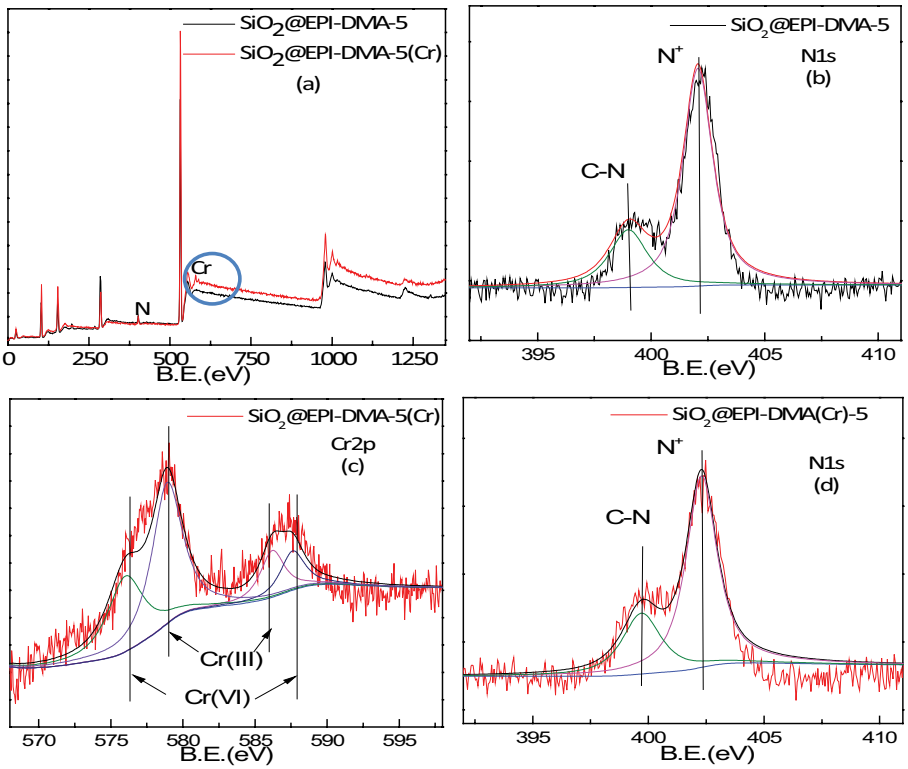

Fig. 7. (a) X-ray spectra of SiO_2@EPI-DMA-5 and SiO_2@EPI-DMA-5(Cr); the high-resolution X-ray N1s spectra of (b) SiO_2@EPI-DMA-5; the high-resolution X-ray Cr2p spctra of (c) SiO_2@EPI-DMA-5(Cr); the high-resolution X-ray N1s spectra of (d) SiO_2@EPI-DMA-5(Cr).

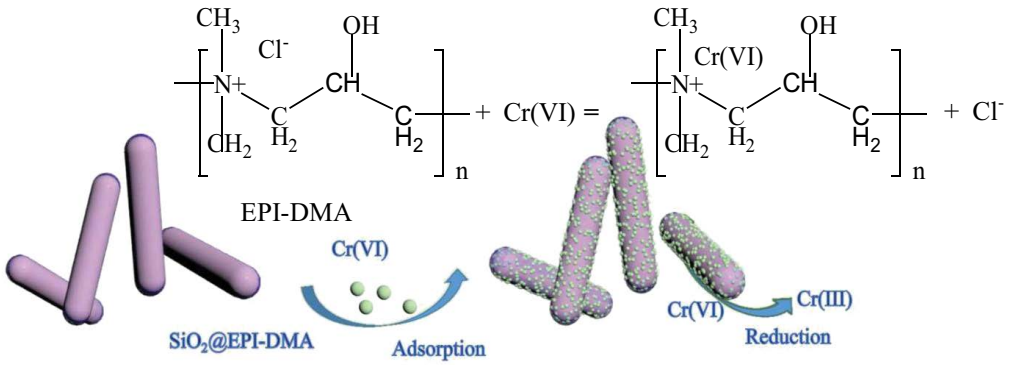

Fig. 8. Proposed adsorption mechanism for Cr(VI) adsorption by SiO_2@EPI-DMA.

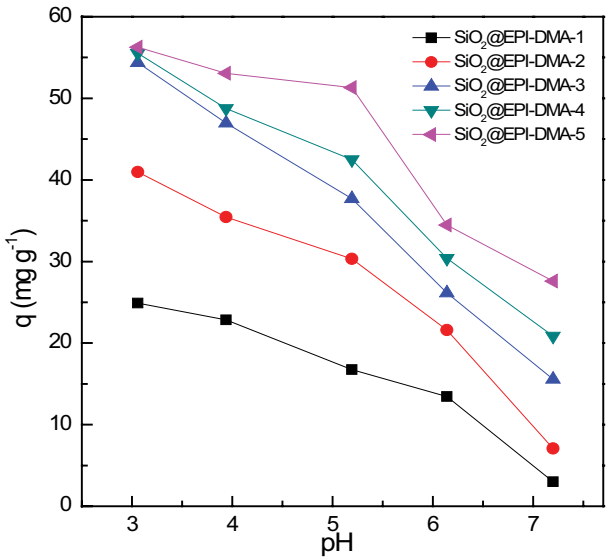

Fig. 9. Cr(VI) equilibrium capacities for SiO_2@EPI-DMA adsorbents under different initial pH (experimental conditions: dosages: 0.5 g/L; concentration of Cr(VI): 25 mg/L; contact time: 24 h; temperature = 25°C; 150 rpm).

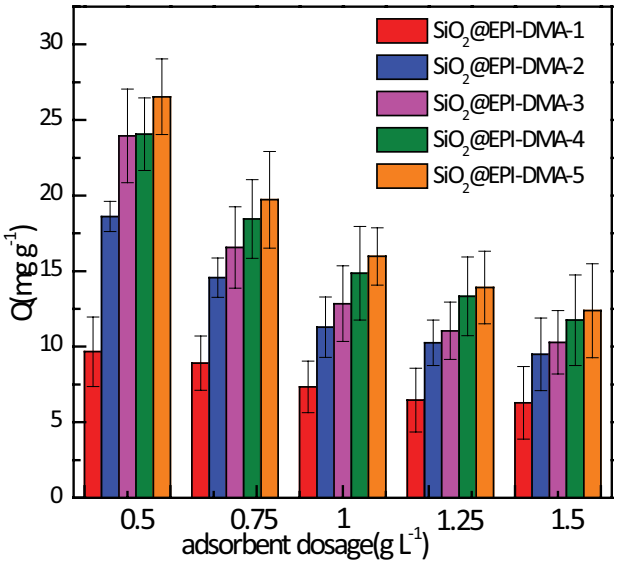

Fig. 10. Adsorption capacity under the different adsorbent dosage (experimental conditions: concentration of Cr(VI): 25 mg/L; contact time: 24 h; temperature = 25°C; 150 rpm; pH = 3.0).

The adsorption capacities decreased remarkably when pH was raised from 3.0 to 7.0, and the maximum equilibrium capacities were all obtained at pH 3.0. In lower pH solution, the plenty of H^+ made the grafting EPI-DMA highly protonated, which was favorable to the electrostatic interaction with negative Cr(VI) and the more grafting positive EPI-DMA. At higher pH conditions, the increased number of OH^- decreased the degree of protonation. And the excessive OH^- increased competition with $Cr_2O_7^{2-}$ or $HCrO_4^-$ for the active sites on SiO_2@EPI-DMA adsorbents. Therefore the Cr(VI) equilibrium capacities decreased with the pH of the solution increased.

3.3.2. Effect of the dosage on Cr(VI) adsorption

Cr(VI) adsorption capacity at different SiO_2@EPI-DMA dosages is as shown in Fig. 10. The pH, concentration of Cr(VI), contact time and adsorption temperature were kept at 3.0, 25 mg/L, 24 h and 25°C, respectively. SiO_2@EPI-DMA dosages were ranged from 0.5 to 1.5 g/L. The Cr(VI) adsorption capacity on SiO_2@EPI-DMA-5 declined from 27 to 12 mg/g when the adsorbent dosages increased. The amount of Cr(VI) ion was certain in the solution of 25 mg/L Cr(VI). With the increase of adsorbent dosage, the amount of chromium ions assigned to the unit sorbent decreased, which made the adsorption capacity decreased. As a result, a dosage of 0.5 g/L was suitable for use in the subsequent adsorption tests.

3.3.3. Adsorption isotherms for Cr(VI) adsorption

The isotherms models reflected the adsorption capacity of SiO_2@EPI-DMA and the interaction between SiO_2@EPI-DMA and Cr(VI). In this research, the data obtained from various samples at 25°C were depicted by two different isotherms: Freundlich Eq. (3) and Langmuir Eq. (4) models [41]. The adsorption isotherm expressions can be presented as follows:

$$q_e = K_F C_e^{1/n} \tag{3}$$

$$q_e = \frac{q_m K_L C_e}{1 + K_L C_e} \tag{4}$$

where C_e (mg/L) and q_e (mg/g) are the equilibrium concentration and adsorption capacity; q_m (mg/g) is the maximum adsorption capacity calculated by the Langmuir model; K_F (mg/g(L/mg)$^{1/n}$) and n are Freundlich constants which are related to the capacity and intensity; K_L (L/mg) is the Langmuir constant.

The free energy parameters (ΔG) of adsorption were calculated by the following formula [33], which could be useful for understanding the adsorption. R is the ideal gas constant; T is the adsorption temperature; K_0 is thermodynamics equilibrium constant, which can be obtained the intercept of the linear plot of $\ln Q_e/C_e$ vs. C_e. The free energy was calculated as –10.4058, –12.8466, –16.3991, –17.4698, –18.0031 for SiO_2@EPI-DMA-1, SiO_2@EPI-DMA-2, SiO_2@EPI-DMA-3, SiO_2@EPI-DMA-4 and SiO_2@EPI-DMA-5, respectively. The values of ΔG were less than 0, which indicated that the adsorption could happen spontaneously.

$$\Delta G = -RT \ln K_0 \tag{5}$$

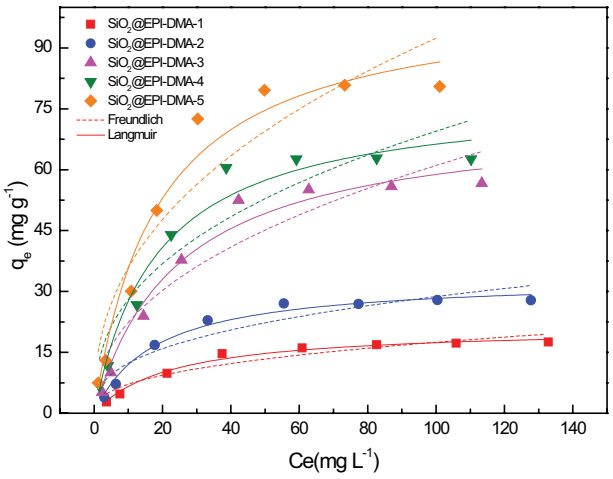

Fig. 11. Adsorption isotherms of Cr(VI) onto different SiO_2@EPI-DMA samples (dosages: 0.5 g L^{-1}; contact time: 24 h; temperature = 25°C; 150 rpm).

Fig. 11 shows the fitting of adsorption isotherms. The isotherms parameters are summarized in Table 2. The R_L^2 values were higher than R_F^2 for all SiO_2@EPI-DMA adsorbents, suggesting that the experimental isotherm data were better fitted by the Langmuir model and Cr(VI) adsorption occurred at specific homogeneous sites over mono-layer pattern [42]. According to the Langmuir model, the maximum adsorption capacities of Cr(VI) adsorbed were calculated as 21.25, 33.31, 73.13, 78.49 and 102.7 mg/g for SiO_2@EPI-DMA-1, SiO_2@EPI-DMA-2, SiO_2@EPI-DMA-3, SiO_2@EPI-DMA-4 and SiO_2@EPI-DMA-5, respectively. As a result, the increased adsorption capacity was well consistent with the grafting amounts of EPI-DMA.

Table 3 shows a comparison of different adsorbents for Cr(VI) adsorption. It is obvious that the Cr(VI) adsorption of SiO_2@EPI-DMA-5 was higher than other relevant adsorbents. Consequently, EPI-DMA is a good functional reagent for SiO_2 and the SiO_2@EPI-DMA-5 has presented promising application for Cr(VI) removal.

3.3.4. Adsorption kinetics for Cr(VI) adsorption

To further study the adsorption kinetics of Cr(VI) onto SiO_2@EPI-DMA, pseudo-first-order (Eq. (6)), pseudo-second-order (Eq. (7)) and intra-particle diffusion (Eq. (8)) [40], are presented as follows:

$$\ln\left(q_e - q_t\right) = \ln q_e - k_1 t \tag{6}$$

$$\frac{t}{q_t} = \frac{1}{k_2 q_e^2} + \frac{1}{q_e} t \tag{7}$$

Table 3
Adsorption comparison of SiO_2@EPI-DMA-5 and reported adsorbents for Cr(VI)

Adsorption	q_m (mg/g)	References
SiO_2@EPI-DMA-5	102.7	This study
Commercial activated carbon	27.8	[43]
Coconut-coir activated carbon	38.5	[43]
Fe-coated cotton stalk biochar	67.44	[44]
SKN1 resins	46.34	[45]
$MnFe_2O_4$@SiO_2-CTAB	25	[46]

Table 2
Parameters of adsorption isotherms for adsorption of Cr(VI) onto SiO_2@EPI-DMA

Sample	Freundlich model			Langmuir model		
	1/n	K_f[(mg/g)(1/mg)$^{1/n}$]	R_F^2	q_m (mg/g)	K_L (L/mg)	R_L^2
SiO_2@EPI-DMA-1	0.3888	2.916	0.8967	21.25	0.04	0.9946
SiO_2@EPI-DMA-2	0.3679	5.282	0.8717	33.31	0.05	0.9982
SiO_2@EPI-DMA-3	0.4359	8.201	0.8871	73.13	0.04	0.9897
SiO_2@EPI-DMA-4	0.3944	11.31	0.8715	78.49	0.05	0.9835
SiO_2@EPI-DMA-5	0.4105	13.95	0.8739	102.7	0.05	0.9805

$$q_t = k_{pi} t^{1/2} + C \quad (8)$$

where q_e and q_t (mg/g) are the adsorption capacity of Cr(VI) at different adsorption reaction time t (min), respectively; k_1 (min^{-1}), k_2 (g mg^{-1} min^{-1}) and k_{pi} are the rate constant of the kinetic models.

The adsorption kinetics models and parameters are presented in Fig. 12 and Table 4. Based on the results, the R^2 values (0.9997–0.9999) of pseudo-second-order were higher than those (0.8714–0.9195) of pseudo-first-order. Therefore, the pseudo-second-order model was more appropriate for depicting the Cr(VI) adsorption, which further revealed that chemisorption existed in the adsorption process. As shown in Fig. 12c, the adsorption curves of intra-particle diffusion model were divided into two linear parts, which further indicated that two steps were involved in the Cr(VI) adsorption process by the SiO_2@EPI-DMA. The first linear parts revealed that the Cr(VI) diffused on the exterior surface of the adsorbent. The rates of the first stage were much higher, which was momentary adsorption owing to abundantly available active sites and functional groups as strong electrostatic force. The rates of second linear parts were flat due to that the active sites were gradually saturated, which represented the Cr(VI) equilibrium of adsorption.

3.3.5. Desorption and regeneration study for Cr(VI) adsorption

The regeneration of SiO_2@EPI-DMA adsorbent was also examined for the sake of the feasible and economic adsorption process. The adsorbed SiO_2@EPI-DMA was put into 0.1 M HCl solution to desorb chromium ions, and soaking for 12 h. Then regeneration of SiO_2@EPI-DMA was prepared by filtering and drying. The adsorption conditions of the regeneration of SiO_2@EPI-DMA were 25 mg/L Cr(VI), pH = 3.0 and 0.5 g/L dosage. Fig. 13 illustrates that the desorption efficiency was 60% after five desorption regeneration cycles. The result validated the recyclability of SiO_2@EPI-DMA for Cr(VI) adsorption.

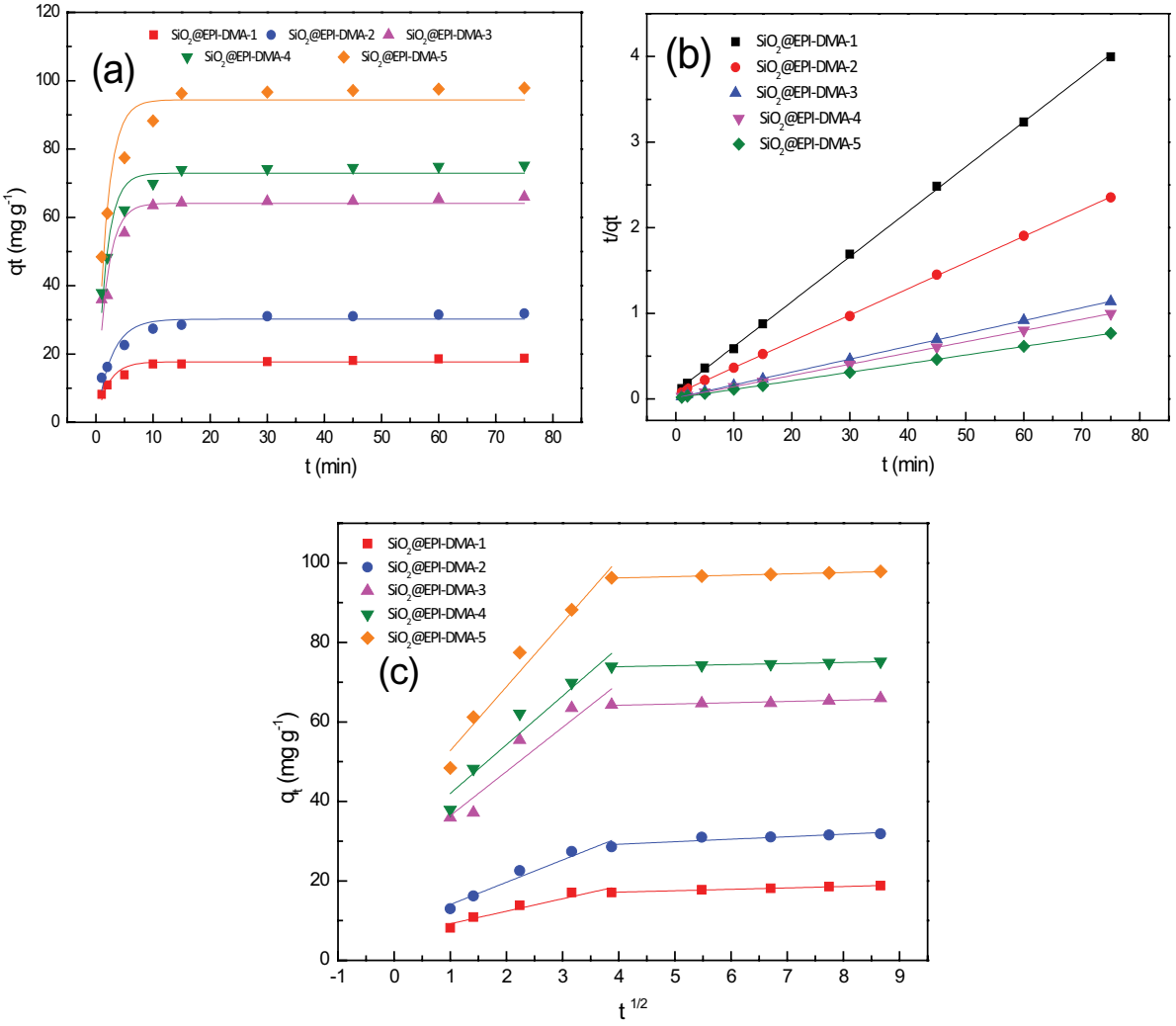

Fig. 12. (a) Pseudo-first-order, (b) pseudo-second-order and (c) intra-particle diffusion model for adsorption of Cr(VI) on SiO_2@EPI-DMA.

Table 4
Parameters of pseudo-first-order, pseudo-second-order and intra-particle diffusion model

Kinetic models	Parameters	Absorbent				
		SiO_2@EPI-DMA-1	SiO_2@EPI-DMA-2	SiO_2@EPI-DMA-3	SiO_2@EPI-DMA-4	SiO_2@EPI-DMA-5
Pseudo-first-order model	k_1 (min^{-1})	0.47	0.37	0.55	0.58	0.55
	$q_{e,cal}$ (mg/g)	17.71	30.19	64.11	72.93	94.38
	R^2	0.9041	0.9032	0.8714	0.9195	0.8878
Pseudo-second-order model	k_2 (g/mg min)	0.032	0.016	0.016	0.014	0.009
	$q_{e,cal}$ (mg/g)	19.1	32.6	66.6	76.2	99.4
	R^2	0.9997	0.9998	0.9998	0.9999	0.9998
Intra-particle diffusion model	k_{1d}	3.15	5.61	11.11	12.27	16.09
	C_1	6.07	8.44	25.31	29.74	36.68
	R_1^2	0.9059	0.9441	0.8808	0.9192	0.9536
	k_{2d}	0.35	0.63	0.32	0.27	0.34
	C_2	15.75	26.72	62.93	72.84	94.87
	R_2^2	0.9929	0.9928	0.9935	0.9946	0.9917

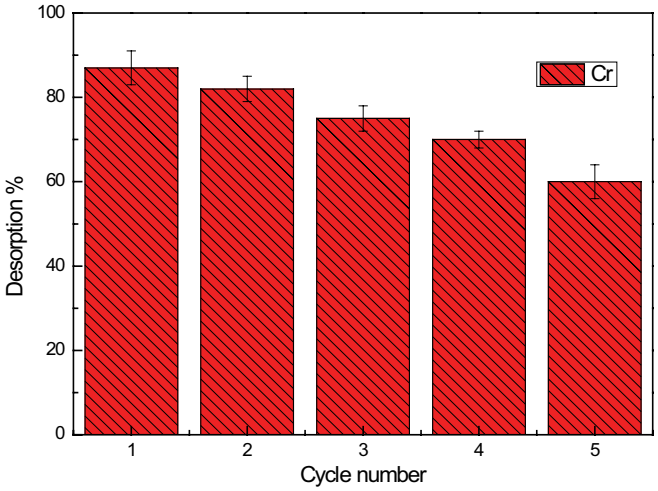

Fig. 13. Desorption efficiency of SiO_2@EPI-DMA in regeneration tests.

4. Conclusions

SiO_2@EPI-DMA adsorbents were successfully prepared by the sonochemical in situ modification for enhanced Cr(VI) adsorption. SiO_2@EPI-DMA prepared at different concentrations of cationic EPI-DMA exhibited different physicochemical characteristics and adsorptive properties. It was found that the improved adsorption capacity corresponded well to the amount of grafted functional ammonium groups after the EPI-DMA modification. The optimal processing temperature and EPI-DMA concentration were designed to be 25°C and 15%, respectively. The adsorption capacity of SiO_2@EPI-DMA showed the maximum Cr(VI) capacity occurred at 102.7 mg/g. The equilibrium data were well fitted by the Langmuir model. The adsorption kinetics was better depicted by the pseudo-second-order. These results demonstrated that the prepared SiO_2@EPI-DMA could be a promising adsorbent for Cr(VI) removal.

Acknowledgments

The authors would like to extend their thanks to the support by Tai Shan Scholar Foundation (No. ts201511003) and the Major technological innovation engineering project of Shandong Province (No. 2018CXGC1010).

References

[1] Y.C. Sharma, Cr(VI) removal from industrial effluents by adsorption on an indigenous low-cost material, Colloids Surf., A, 215 (2003) 155–162.
[2] S. Chen, Q.Y. Yue, B.Y. Gao, Q. Li, X.X. Xu, K. Fu, Adsorption of hexavalent chromium from aqueous solution by modified corn stalk: a fixed-bed column study, Bioresour. Technol., 113 (2012) 114–120.
[3] A.D. Bokare, W. Choi, Advanced oxidation process based on the Cr(III)/Cr(VI) redox cycle, Environ. Sci. Technol., 45 (2011) 9332–9338.
[4] B. Xie, C. Shan, Z. Xu, X. Li, X. Zhang, J. Chen, B. Pan, One-step removal of Cr(VI) at alkaline pH by UV/sulfite process: reduction to Cr(III) and in situ Cr(III) precipitation, Chem. Eng. J., 308 (2017) 791–797.
[5] Y. Li, Q.Y. Yue, B.Y. Gao, Q. Li, C. Li, Adsorption thermodynamic and kinetic studies of dissolved chromium onto humic acids, Colloids Surf., B, 65 (2008) 25–29.
[6] W. Cai, M. Gu, W. Jin, J. Zhou, CTAB-functionalized C@SiO_2 double-shelled hollow microspheres with enhanced and selective adsorption performance for Cr(VI), J. Alloys Comp., 777 (2019) 1304–1312.
[7] W. Cai, J. Wei, Z. Li, Y. Liu, J. Zhou, B. Han, Preparation of amino-functionalized magnetic biochar with excellent adsorption performance for Cr(VI) by a mild one-step hydrothermal method from peanut hull, Colloids Surf. A, 563 (2019) 102–111.
[8] K. Gong, Q. Hu, Y. Xiao, X. Cheng, H. Liu, N. Wang, B. Qiu, Z. Guo, Triple layered core-shell ZVI@carbon@polyaniline composite enhanced electron utilization in Cr(VI) reduction, J. Mater. Chem. A, 6 (2018) 11119–11128.
[9] Y. Jiang, W. Cai, W. Tu, M. Zhu, Facile cross-link method to synthesize magnetic Fe_3O_4@SiO_2-chitosan with high adsorption capacity toward hexavalent chromium, J. Chem. Eng. Data, 64 (2019) 226–233.
[10] J. Lee, J.H. Kim, K. Choi, H.G. Kim, J.A. Park, S.H. Cho, S.W. Hong, J.H. Lee, Investigation of the mechanism of chromium removal in (3-aminopropyl)trimethoxysilane functionalized mesoporous silica, Sci. Rep., 8 (2018) 12078.

[11] S. Shariati, M. Khabazipour, F. Safa, Synthesis and application of amine functionalized silica mesoporous magnetite nanoparticles for removal of chromium(VI) from aqueous solutions, J. Porous Mater., 24 (2017) 129–139.
[12] C.E. Barrera-Diaz, V. Lugo-Lugo, B. Bilyeu, A review of chemical, electrochemical and biological methods for aqueous Cr(VI) reduction, J. Hazard. Mater., 223–224 (2012) 1–12.
[13] Z.F. Ren, X.X. Xu, X. Wang, B.Y. Gao, Q.Y Yue, W. Song, L. Zhang, H. Wang, FTIR, Raman, and XPS analysis during phosphate, nitrate and Cr(VI) removal by amine cross-linking biosorbent, J. Colloid Interface Sci., 468 (2016) 313–323.
[14] J. Ren, P. Hao, W. Sun, R. Shi, S. Liu, Ordered mesoporous silica-carbon-supported copper catalyst as an efficient and stable catalyst for catalytic oxidative carbonylation, Chem. Eng. J., 328 (2017) 673–682.
[15] J.A. Sullivan, R. Herron, A.D. Phillips, Towards an understanding of the beneficial effect of mesoporous materials on the dehydrogenation characteristics of NH_3 BH_3, Appl. Catal., B, 201 (2017) 182–188.
[16] M. Geszke-Moritz, M. Moritz, Modeling of boldine alkaloid adsorption onto pure and propyl-sulfonic acid-modified mesoporous silicas. A comparative study, Mater. Sci. Eng. C Mater. Biol. Appl., 69 (2016) 815–830.
[17] B. Li, J. Ma, L. Zhou, Y. Qiu, Magnetic microsphere to remove tetracycline from water: adsorption, H_2O_2 oxidation and regeneration, Chem. Eng. J., 330 (2017) 191–201.
[18] G. Mohammadnezhad, S. Abad, R. Soltani, M. Dinari, Study on thermal, mechanical and adsorption properties of amine-functionalized MCM-41/PMMA and MCM-41/PS nanocomposites prepared by ultrasonic irradiation, Ultrason. Sonochem., 39 (2017) 765–773.
[19] V.H.A. Pinto, J.S. Rebouças, G.M. Ucoski, E.H. de Faria, B.F. Ferreira, R.A. Silva San Gil, S. Nakagaki, Mn porphyrins immobilized on non-modified and chloropropyl-functionalized mesoporous silica SBA-15 as catalysts for cyclohexane oxidation, Appl. Catal., A, 526 (2016) 9–20.
[20] S. Hao, A. Verlotta, P. Aprea, F. Pepe, D. Caputo, W. Zhu, Optimal synthesis of amino-functionalized mesoporous silicas for the adsorption of heavy metal ions, Microporous Mesoporous Mater., 236 (2016) 250–259.
[21] A. Shahat, H.M.A. Hassan, H.M.E. Azzazy, E.A. El-Sharkawy, H.M. Abdou, M.R. Awual, Novel hierarchical composite adsorbent for selective lead (II) ions capturing from wastewater samples, Chem. Eng. J., 332 (2018) 377–386.
[22] Z.Y. Kong, J.F. Wei, Y.H. Li, N.N. Liu, H. Zhang, Y. Zhang, L. Cui, Rapid removal of Cr(VI) ions using quaternary ammonium fibers functioned by 2-(dimethylamino)ethyl methacrylate and modified with 1-bromoalkanes, Chem. Eng. J., 254 (2014) 365–373.
[23] C. Zhou, Q. Wu, T. Lei, Negulescu II, Adsorption kinetic and equilibrium studies for methylene blue dye by partially hydrolyzed polyacrylamide/cellulose nanocrystal nanocomposite hydrogels, Chem. Eng. J., 251 (2014) 17–24.
[24] J. Zhu, K. Kailasam, X. Xie, R. Schomaecker, A. Thomas, High-surface-area SBA-15 with enhanced mesopore connectivity by the addition of poly(vinyl alcohol), Chem. Mater., 23 (2011) 2062–2067.
[25] Q. Li, Q.Y. Yue, Y. Su, B.Y. Gao, Equilibrium and a two-stage batch adsorber design for reactive or disperse dye removal to minimize adsorbent amount, Bioresour. Technol., 102 (2011) 5290–5296.
[26] Q. Li, Q.Y. Yue, H.J. Sun, Y. Su, B.Y. Gao, A comparative study on the properties, mechanisms and process designs for the adsorption of non-ionic or anionic dyes onto cationic-polymer/bentonite, Environ. Manage., 91 (2010) 1601–1611.
[27] J.R. Deka, S. Vetrivel, H.Y. Wu, Y.C. Pan, C.C. Ting, Y.L. Tsai, H.M. Kao, Rapid sonochemical synthesis of MCM-41 type benzene-bridged periodic mesoporous organosilicas, Ultrason. Sonochem., 21 (2014) 387–394.
[28] H. Liu, S. Ji, H. Yang, H. Zhang, M. Tang, Ultrasonic-assisted ultra-rapid synthesis of monodisperse meso-SiO_2@Fe_3O_4 microspheres with enhanced mesoporous structure, Ultrason. Sonochem., 21 (2014) 505–512.
[29] S. Mallakpour, H.Y. Nazari, Ultrasonic-assisted fabrication and characterization of PVC-SiO_2 nanocomposites having bovine serum albumin as a bio coupling agent, Ultrason. Sonochem., 39 (2017) 686–697.
[30] R. Soltani, M. Dinari, G. Mohammadnezhad, Ultrasonic-assisted synthesis of novel nanocomposite of poly(vinyl alcohol) and amino-modified MCM-41: a green adsorbent for Cd(II) removal, Ultrason. Sonochem., 40 (2018) 533–542.
[31] Y.L. Verma, A.K. Gupta, R.K. Singh, S. Chandra, Preparation and characterisation of ionic liquid confined hybrid porous silica derived from ultrasonic assisted non-hydrolytic sol–gel process, Microporous Mesoporous Mater., 195 (2014) 143–153.
[32] K.L. Seon, J. Jin, H.W. Taeghwan, L. HoIo, Rapid sonochemical synthesis of spherical-shaped mesoporous SBA-15 silica and Ti-incorporated SBA-15 silica materials, Ind. Eng. Chem., 91 (2003) 83–88.
[33] Q.Y. Yue, Q. Li, B.Y. Gao, A.J. Yuan, Y. Wang, Formation and characteristics of cationic-polymer/bentonite complexes as adsorbents for dyes, Appl. Clay Sci., 35 (2007) 268–275.
[34] A. Bibi, H. Ju, Efficient enrichment of glycopeptides with sulfonic acid-functionalized mesoporous silica, Talanta, 161 (2016) 681–685.
[35] C. Chen, X. Wang, L. Zhang, X. Zou, W. Ding, X. Lu, Synthesis of mesoporous Ni–La_2O_3/SiO_2 by ploy(ethylene glycol)-assisted sol-gel route as highly efficient catalysts for dry reforming of methane with a H_2/CO ratio of unity, Catalysis Commun., 94 (2017) 38–41.
[36] J. Zhu, X. Zhu, J. Gu, L. Zhao, L. Jiang, Y. Qiu, Effective adsorption and concentration of carnosine by nickel species within mesoporous silica, LWT - Food Sci. Technol., 74 (2016) 211–218.
[37] H.H.P. Yiu, C.H. Botting, N.P. Botting, P.A. Wright, Size selective protein adsorption on thiol-functionalised SBA-15 mesoporous molecular sieve, Phys. Chem. Chem. Phys., 3 (2001) 2983–2985.
[38] B.K. Sodipo, A.A. Aziz, One minute synthesis of amino-silane functionalized superparamagnetic iron oxide nanoparticles by sonochemical method, Ultrason. Sonochem., 40 (2018) 837–840.
[39] N. Li, Q. Yue, B. Gao, X. Xu, Y. Kan, P. Zhao, Magnetic graphene oxide functionalized by poly dimethyl diallyl ammonium chloride for efficient removal of Cr(VI), J. Taiwan Inst. Chem. Eng., 91 (2018) 499–506.
[40] S. Chen, Q.Y. Yue, B.Y. Gao, Q. Li, X.X. Xu, Removal of Cr(VI) from aqueous solution using modified corn stalks: characteristic, equilibrium, kinetic and thermodynamic study, Chem. Eng. J., 168 (2011) 909–917.
[41] Q. Li, Q.Y Yue, Y. Su, B.Y. Gao, H.J. Sun, Equilibrium, thermodynamics and process design to minimize adsorbent amount for the adsorption of acid dyes onto cationic polymer-loaded bentonite, Chem. Eng. J., 158 (2010) 489–497.
[42] R. Khosravi, G. Moussavi, M.T. Ghaneian, M.H. Ehrampoush, B. Barikbin, A.A. Ebrahimi, G. Sharifzadeh, Chromium adsorption from aqueous solution using novel green nanocomposite: adsorbent characterization, isotherm, kinetic and thermodynamic investigation, J. Mol. Liq., 256 (2018) 163–174.
[43] M. Chaudhuri, N.K. Bin Azizan, Adsorptive removal of chromium(VI) from aqueous solution by an agricultural waste-based activated carbon, Water Air Soil Pollut., 223 (2012) 1765–1771.
[44] S.B. Duan, W. Ma, Y.Z. Pan, F.Q. Meng, S.G. Yu, L. Wu, Synthesis of magnetic biochar from iron sludge for the enhancement of Cr (VI) removal from solution, J. Taiwan Inst. Chem. Eng., 80 (2017) 835–841.
[45] S. Rengaraj, K.H. Yeon, S.H. Moon, Removal of chromium from water and wastewater by ion exchange resins, J. Hazard. Mater., 87 (2001) 273–287.
[46] N. Li, F.L. Fu, J.W. Lu, Z.C. Ding, B. Tang, J.B. Pang, Facile preparation of magnetic mesoporous $MnFe_2O_4$@SiO_2-CTAB composites for Cr(VI) adsorption and reduction, Environ. Pollut., 220 (2017) 1376–1385.